A PARALLEL SOLVER FOR REACTION-DIFFUSION SYSTEMS IN COMPUTATIONAL ELECTROCARDIOLOGY

PIERO COLLI-FRANZONE * AND LUCA F. PAVARINO †

Abstract. In this work, a parallel three-dimensional solver for numerical simulations in computational electrocardiology is introduced and studied. The solver is based on the anisotropic Bidomain cardiac model, consisting of a system of two degenerate parabolic reaction-diffusion equations describing the intra and extracellular potentials of the myocardial tissue. This model includes intramural fiber rotation and anisotropic conductivity coefficients that can be fully orthotropic or axially symmetric around the fiber direction. The solver also includes the simpler anisotropic Monodomain model, consisting of only one reaction-diffusion equation. These cardiac models are coupled with a membrane model for the ionic currents, consisting of a system of ordinary differential equations that can vary from the simple FitzHugh-Nagumo (FHN) model to the more complex phase-I Luo-Rudy model (LR1). The solver employs structured isoparametric Q_1 finite elements in space and a semi-implicit adaptive method in time. Parallelization and portability are based on the PETSc parallel library. Large-scale computations with up to $O(10^7)$ unknowns have been run on parallel computers, simulating excitation and repolarization phenomena in three-dimensional domains.

Key words. reaction-diffusion equations; bidomain model; finite elements; parallel solver

AMS Subject Classification: 65M60, 65M55

1. Introduction. The bioelectric activity of the heart is the subject of a vast interdisciplinary literature in medicine, bioengineering, mathematical biology, physiology, chemistry and physics; see the reference books by Zipes and Jalife [66, Part V and VII], Panfilov and Holden [38], Keener and Sneyd [30] and the references therein. Computational studies and numerical simulations have played an important role in electrocardiology. Due to the difficulty of direct measurements, many experimental studies have been coupled with numerical investigations, even in medical and bioengineering works.

Particularly intense has been the computational study of reentry phenomena and their relationships with myocardial arrhythmias; see e.g. the recent journal special issues [1, 2, 3] and the references therein.

The most complete model of cardiac electrical activity is the Bidomain model, see eg. [49, 23]. It consists of a system of two degenerate parabolic reaction-diffusion equations describing the intra and extracellular potential in the cardiac muscle, coupled with a system of ordinary differential equations describing the ionic currents flowing through the cellular membrane. This model is computationally expensive because of the involvement of different space and time scales. In fact, meaningful portions of cardiac tissue have sizes on the order of centimeters, while the steep potential gradient is localized in a thin layer about one millimiter thick, requiring discretizations on the order of a tenth of millimiter. Moreover, a normal heartbeat can last on the order of one second, while the time constants of the rapid kinetics involved range from 0.1 to 500 milliseconds, requiring in some phases time steps on the order of the hundredths of milliseconds (or less when currents or shocks are applied). Therefore, in realistic three-dimensional models it is possible to have discrete problems with more than $O(10^7)$ unknowns at every time step and simulations have to be run for many thousands of time steps.

A simplified cardiac tissue model is the anisotropic Monodomain system, i.e. a parabolic reaction-diffusion equation describing the evolution of the transmembrane potential coupled with an ionic model. This model has been widely used for three-dimensional simulations considering ionic models ranging from simple FitzHugh-Nagumo (FHN) variants (Winfree

*Department of Mathematics, Università di Pavia, Via Ferrata 1, 27100 Pavia, Italy. E-mail address: colli@imati.cnr.it. This work was supported by MURST (PRIN "Numerical Modelling for Scientific Computing and Advanced Applications") and by CNR-Agenzia 2000 "Computational Grids and Applications".

†Department of Mathematics, Università di Milano, Via Saldini 50, 20133 Milano, Italy. E-mail adress: Luca.Pavarino@mat.unimi.it. This work was supported by MURST (PRIN "Numerical Modelling for Scientific Computing and Advanced Applications").

[62, 63], Rogers and McCulloch [47], Panfilov [37]) to the more complex phase-I Luo-Rudy (LR1) model [32], see e.g. Efimov et al. [19], Rappel [46], Garfinkel et al. [21].

Previous Bidomain computations, mainly focusing on the excitation phase, were performed on medium scale problems by Colli-Franzone [12], Roth [48], Hooke et al. [26], Henriquez et al. [23, 24], Muzikant et al. [34]. These Bidomain studies of the excitation phase, were able to reproduce the qualitative patterns and morphologies of the experimentally observed extracellular potential maps and electrograms (see e.g. Taccardi et al. [56], Colli-Franzone et al. [14, 15], Henriquez et al. [24], Muzikant et al. [34]).

A further reduction of the computational complexity of the simulation of the excitation phase has been achieved by solving simplified kinematic models, called eikonal equations, describing the motion of the excitation wave fronts, see e.g. Colli-Franzone et al. [12], Keener [28] and Bellettini et al. [8]. On the other hand, simplified approaches derived from reaction-diffusion models are not available at present for the description of all the phases of an entire heartbeat.

Large-scale simulations of the whole heartbeat using Bidomain and Monodomain models require adaptive and parallel tools in order to reduce their high computational cost. While both tools can in principle be applied to both space and time, we have chosen to use adaptive methods in time and parallel solvers in space, since the other alternatives are still the subject of current research even for simpler model problems in two dimensions (Cherry et al. [11], Quan et al. [44], Moore [33], Yu [65, 64], Pennacchio [39]). Therefore in this paper, we introduce and study a parallel solver for the Bidomain system, employing an adaptive time-stepping strategy that efficiently deals with the three main phases (depolarization, plateau, repolarization) of a complete heartbeat. In order to change the time-step size in these different phases without stability constraints associated with the space discretization of the diffusive part of the system, we must treat the latter implicitly. Therefore, we use a semi-implicit method in time, where the reaction terms are treated explicitly and the diffusion terms implicitly. The space discretization is based on structured isoparametric Q_1 finite elements. Parallelization and portability are based on the PETSc parallel library [6, 7] and on using a preconditioned conjugate gradient solver at each time step. We apply the parallel solver in order to simulate a full heartbeat in a model of cardiac tissue which includes intramural fiber rotation and anisotropic conductivity coefficients of the intra and extracellular media, than can be fully orthotropic or axially symmetric around the fiber direction.

The rest of the paper is organized as follows. In Sections 2 and 3, we briefly review the anisotropic Bidomain and Monodomain models respectively. In Section 4, we introduce the basic elements of the membrane models describing the ionic currents. In Section 5, the Bidomain and Monodomain models are written in variational form and some references to the available mathematical analysis are given. In Section 6, we discretize in space the continuous models by isoparametric finite elements, while an adaptive semi-implicit discretization in time is given in Section 7. In Section 8, we describe our parallel implementation based on the PETSc parallel library. In Section 9, several results of numerical experiments with our parallel solver are presented, varying both the cardiac tissue model (from Monodomain to Bidomain) and the ionic model (from FHN variants to the LR1 model), on cartesian slabs and ellipsoidal domains. Finally, some concluding remarks are presented in Section 10.

2. The macroscopic Bidomain model. At the microscopic level, the cellular structure of the cardiac tissue consists of elongated cardiac cells surrounded by extracellular space (including collagene matrix and blood vessel network) and connected by end-to-end and/or side-to-side junctions. Starting from a microscopic model of this discrete cellular structure, it is possible to derive, by a homogenization process, a macroscopic model for a periodic assembling; see Neu and Krassowska [35], Keener and Sneyd [30], Colli-Franzone and Savaré [17] for a formal derivation and modeling details. The resulting macroscopic Bidomain model is a representation of the cardiac tissue as the superposition of two anisotropic continuous media, the intra (i) and extra (e) cellular media, coexisting at every point of the tissue and

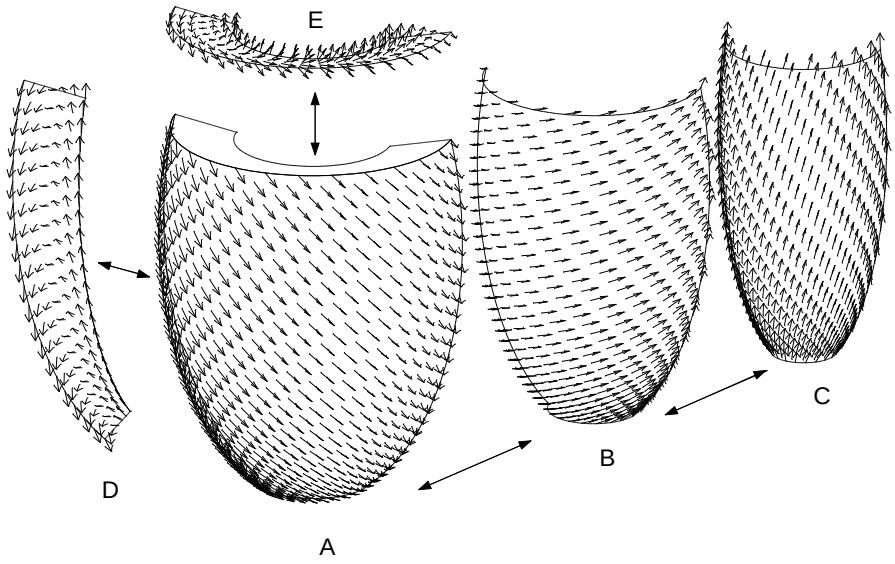

FIG. 2.1. *Fiber direction on epicardium (A), a mid-wall layer (B), endocardium (C), a meridian section (D) and a transverse section (E)*

connected by a distributed continuous cellular membrane. This macroscopic model describes the averaged intra and extracellular electric potentials and currents by a reaction-diffusion system of degenerate parabolic type.

Let $\Omega \subset \mathbf{R}^3$ be the bounded physical region occupied by the cardiac tissue. In the macroscopic Bidomain representation of the cardiac tissue, the anisotropic structure of the two averaged continuous media, the intra and the extracellular medium, are characterized by the conductivity tensors D_i and D_e. The anisotropic conductivity is related to the arrangement of the cardiac fibers, whose direction rotates counterclockwise from the epicardium (outer heart surface) to the endocardium (inner surface); see Figure 2.1. We refer to Streeter [54] and Peskin [41] for an experimental and mathematical study of this fiber structure. Recently Le Grice et al. [31] have shown that the ventricular myocardium may be conceived as a set of muscle sheets running radially from epicardium to endocardium. In this laminar organization, it is possible to identify three distinct principal axes at any point $\mathbf{x}$. Let $\mathbf{a}_l(\mathbf{x})$, $\mathbf{a}_t(\mathbf{x})$, $\mathbf{a}_n(\mathbf{x})$ be a triplet of orthonormal vectors related to the structure of the myocardium at a point $\mathbf{x}$, with $\mathbf{a}_l$ parallel to the local fiber direction and $\mathbf{a}_n$ normal to the muscle sheet. This triplet may depend on the position $\mathbf{x}$ in the myocardium. Let $\sigma_l^{i,e}$, $\sigma_t^{i,e}$, $\sigma_n^{i,e}$ be the conductivity coefficients measured along the corresponding directions. In general, these coefficients may depend on $\mathbf{x}$, but in the following we assume that they are constant, i.e. homogeneous anisotropy. Then the conductivity tensors D_i and D_e, generally dependent on the position $\mathbf{x}$, are given by:

$$D_{i,e}(\mathbf{x}) = \sigma_l^{i,e}\ \mathbf{a}_l(\mathbf{x})\mathbf{a}_l^T(\mathbf{x}) + \sigma_t^{i,e}\ \mathbf{a}_t(\mathbf{x})\mathbf{a}_t^T(\mathbf{x}) + \sigma_n^{i,e}\ \mathbf{a}_n(\mathbf{x})\mathbf{a}_n^T(\mathbf{x}). \tag{2.1}$$

If $\sigma_n^{i,e} = \sigma_t^{i,e}$, we recover the axially isotropic case

$$D_{i,e}(\mathbf{x}) = {\sigma_t}^{i,e} I + ({\sigma_l}^{i,e} - {\sigma_t}^{i,e})\mathbf{a}_l(\mathbf{x})\mathbf{a}_l^T(\mathbf{x}).$$

The biolelectric activity of cardiac cells is due to the flow I_{ion} (per unit area of the membrane surface) of various ionic currents (the most important being sodium, potassium and calcium) through the cellular membrane. Since the membrane behaves as a capacitor, then the total membrane current per unit volume is given by

$$I_m = \chi(C_m \frac{\partial v}{\partial t} + I_{ion}),$$

where $v = u_i - u_e$ is the transmembrane potential, the coefficient χ is the ratio of membrane area per tissue volume, C_m is the surface capacitance of the membrane, and $I_{ion}(v, w)$ is the ionic current described later and depending on the membrane model employed.

Imposing the conservation of currents, i.e. the interchange between the two media must balance the membrane current flow per unit volume, we have $\mathrm{div}\mathbf{J}_i = -\mathrm{div}\mathbf{J}_e = I_m$, where $\mathbf{J}_{i,e} = -D_{i,e}\nabla u_{i,e}$ are the intra and extracellular current densities. Therefore, in the Bidomain model, the intra and extracellular potentials u_i, u_e are modeled by the following reaction-diffusion system of PDEs, coupled with a system of ODEs for M gating variables and ion concentrations modeling the ionic currents, described later. Given an applied current per unit volume $I^{i,e}_{app} : \Omega \times (0,T) \longrightarrow \mathbf{R}$, initial conditions $v_0 : \Omega \longrightarrow \mathbf{R}, w_0 : \Omega \longrightarrow \mathbf{R}^M$, find the intra and extracellular potentials $u_i, u_e : \Omega \times (0,T) \longrightarrow \mathbf{R}$, the transmembrane potential $v = u_i - u_e$ and the gating and concentration variables $w : \Omega \times (0,T) \longrightarrow \mathbf{R}^M$ such that

$$
\left\{
\begin{array}{ll}
\chi C_m \dfrac{\partial v}{\partial t} - \mathrm{div}(D_i \nabla u_i) + \chi I_{ion}(v,w) = I^i_{app} & \text{in } \Omega \times (0,T) \\
-\chi C_m \dfrac{\partial v}{\partial t} - \mathrm{div}(D_e \nabla u_e) - \chi I_{ion}(v,w) = -I^e_{app} & \text{in } \Omega \times (0,T) \\
\dfrac{\partial w}{\partial t} - R(v,w) = 0, \qquad v(\mathbf{x},t) = u_i(\mathbf{x},t) - u_e(\mathbf{x},t) & \text{in } \Omega \times (0,T).
\end{array}
\right. \tag{2.2}
$$

In the following, we assume that the cardiac tissue is insulated, therefore homogeneous Neumann boundary conditions are assigned on $\partial\Omega \times (0,T)$

$$\mathbf{n}^T D_i \nabla u_i = 0, \quad \mathbf{n}^T D_e \nabla u_e = 0.$$

Initial conditions (degenerate for u_i and u_e) are assigned in Ω for $t = 0$

$$v(\mathbf{x},0) = u_i(\mathbf{x},0) - u_e(\mathbf{x},0) = v_0(\mathbf{x}), \quad w(\mathbf{x},0) = w_0(\mathbf{x}). \tag{2.3}$$

Adding the two equations of the system, we have $-\mathrm{div}D_i\nabla u_i - \mathrm{div}D_e\nabla u_e = I^i_{app} - I^e_{app}$. Integrating on Ω and applying the divergence theorem, from the Neumann boundary conditions, we then have the following compatibility condition for the system (2.2) to be solvable:

$$\int_\Omega I^i_{app}\,\mathrm{dx} = \int_\Omega I^e_{app}\,\mathrm{dx}. \tag{2.4}$$

We recall that electric potentials in bounded domains are defined up to an additive constant; in our case u_i and u_e are determined up to the same additive time-dependent constant, while v is uniquely determined. This common constant is related to the choice of a reference potential. A usual choice consists in selecting this constant so that u_e has zero average on Ω, i.e.

$$\int_\Omega u_e\,\mathrm{dx} = 0. \tag{2.5}$$

3. The simplified Monodomain model. Assuming equal anisotropy ratio of the two media, i.e. $D_i = \lambda D_e$ with λ constant, and setting $D = \dfrac{\lambda D_i}{1+\lambda}$ and $I_{app} = \dfrac{\lambda I^i_{app}}{1+\lambda} + \dfrac{I^e_{app}}{1+\lambda}$, then the Bidomain system reduces to the anisotropic Monodomain model consisting in a parabolic reaction-diffusion equation for the transmembrane potential v only

$$
\left\{
\begin{array}{ll}
\chi C_m \dfrac{\partial v}{\partial t} - \mathrm{div}(D(\mathbf{x})\nabla v) + \chi I_{ion}(v,w) = I_{app}, & \text{in } \Omega \times (0,T) \\
\dfrac{\partial w}{\partial t} - R(v,w) = 0 & \text{in } \Omega \times (0,T),
\end{array}
\right. \tag{3.1}
$$

with Neumann boundary conditions for v and initial conditions for v and w. The conductivity tensor in the axial symmetric case is given by

$$D(\mathbf{x}) = \sigma_l \ \mathbf{a}_l(\mathbf{x})\mathbf{a}_l^T(\mathbf{x}) + \sigma_t \ \mathbf{a}_t(\mathbf{x})\mathbf{a}_t^T(\mathbf{x}) + \sigma_n \ \mathbf{a}_n(\mathbf{x})\mathbf{a}_n^T(\mathbf{x}) \quad \text{with} \quad \sigma_{l,t,n} = \frac{\lambda}{1+\lambda}\sigma_{l,t,n}^i.$$

This model has been vastly used in computational electrocardiology because it requires substantially less computational and memory resources than the Bidomain model. Nevertheless, it is not an adequate cardiac model since it is unable to reproduce some patterns and morphology of the experimentally observed extracellular potential maps and electrograms; see Colli-Franzone et al. [14], Henriquez et al. [24], Muzikant et al. [34]. Therefore, unequal anisotropy ratio of the intra and extracellular media cannot be neglected.

4. Membrane models and ionic currents. The first membrane model for ionic currents was given in the celebrated work on nerve action potential by Hodgkin and Huxley [25], work that earned them the Nobel prize in Medicine in 1963. Models of Hodgkin-Huxley type have been later developed for the cardiac action potential. In these models, the ionic current through channels of the membrane, due to the transmembrane potential v and M gating and ionic concentration variables $w := (w_1, \ldots, w_M)$, is given by

$$I_{ion}(v, w) = \sum_{k=1}^{N} G_k(v) \prod_{j=1}^{M} w_j^{p_{j_k}} (v - v_k(w)),$$

where $G_k(v)$ is the membrane conductance, v_k is the reversal potential for the k-th current and p_{j_k} are integers. The dynamics of the gating and concentration variables is described by the system of ODE's

$$\frac{\partial w}{\partial t} = R(v, w), \qquad w(\mathbf{x}, 0) = w_0(\mathbf{x}).$$

If w_j is a gating variable, then the associated right-hand side has a special structure, i.e. $R(v, w) = R_j(v, w_j) = \alpha_j(v)(1 - w_j) - \beta_j(v)(w_j), \quad \alpha_j, \quad \beta_j > 0, \quad 0 \le w_j \le 1$. Many refinements of the original Hodgkin-Huxley model have been proposed by fitting improved experimental data with more complex models. We recall here the models by Beeler-Reuter (1977, N = 4, M = 7), phase-I Luo-Rudy (1991, N = 6, M = 7), phase-II Luo-Rudy (1994, N = 10, M = 7). In this paper, we will consider the phase-I Luo-Rudy (LR1) model (see [32]), consisting of six gating variables $w_1, \cdots, w_6$ and one calcium ionic concentration w_7. The action potential generated with this model is shown in the right panel of Figure 4.1 for both the original model (continuous line) and a variant where the slow inward current I_{si} of the model is scaled by a factor 2/3 (dashed line); see the original paper by Luo and Rudy [32, p. 1503, Table 1] for a complete description of the LR1 model. Figure 4.2 shows the time evolution of the LR1 variables at a given point, over a period of 400 msec.

We remark that during a heartbeat, the time course of the transmembrane potential $v(\mathbf{x}, t)$ at each point of the ventricular tissue, also called action potential, displays mainly three phases having different time scales. The first is related to the excitation phase, also called depolarization, where v undergoes an abrupt temporal change lasting about 2 msec, followed by a fast exponential decay toward a plateau value. The second is the plateau phase, lasting from 40-50 msec to about 400 msec, according to the ionic model used and the type of propagating front considered. In this phase, v varies very little and slowly in comparison with the previous depolarization phase and the cardiac tissue is refractory, i.e. any applied stimulus does not elicit another action potential. The last is the recovery phase, also called repolarization, where v returns to the rest value during a period lasting 20-50 msec, after which the tissue becomes excitable again.

Simplified models of lower complexity (with 1 or 2 gating variables) have been proposed too. The simplest and most used is the FitzHugh-Nagumo (FHN) model (N = 1, M = 1).

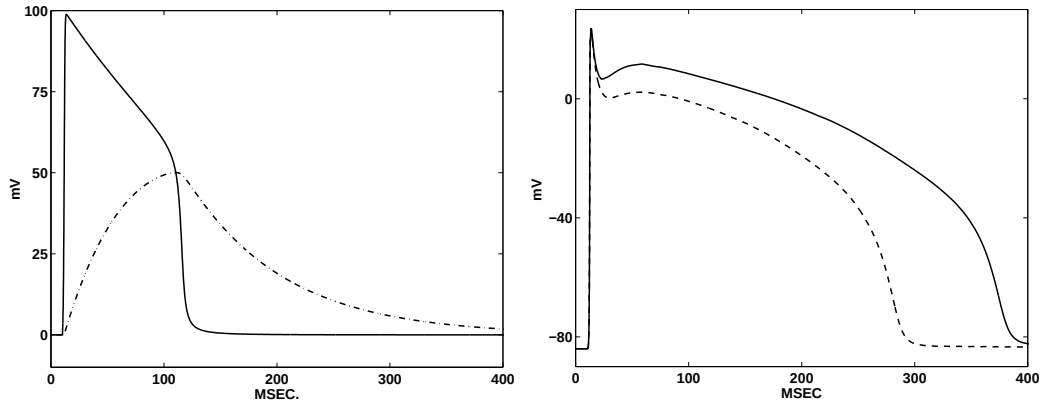

FIG. 4.1. *Action potentials at a given point as a function of time. Left: Rogers-McCulloch FHN variant; action potential (–) and recovery variable (- ·) magnified by a factor 100. Right: original LR1 model (–), LR1 model with I_{si} current scaled by a factor 2/3 (– –)*

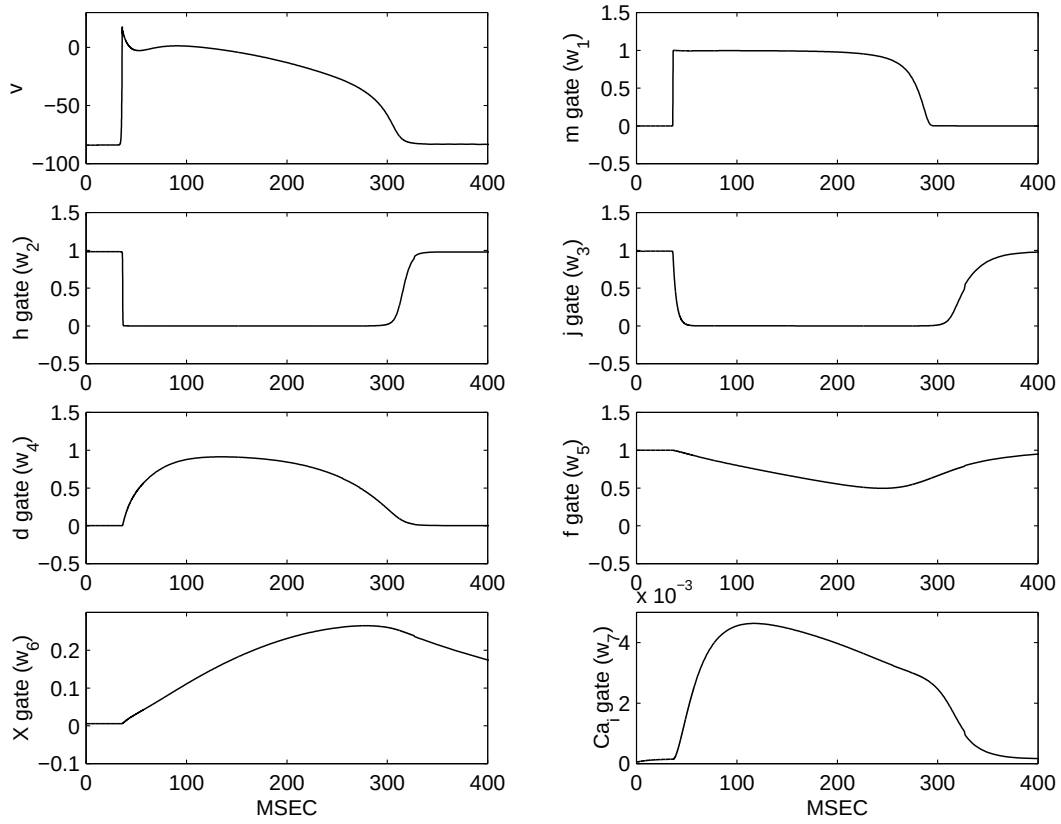

FIG. 4.2. *LR1 membrane model: action potential v, gating variables $w_1, \cdots, w_6$, calcium concentration w_7 at a given point as a function of time*

Assuming that at rest the potential v is zero, in this model the ionic current is described using only one recovery variable w

$$I_{ion}(v, w) = g(v) + \beta w,$$

where $\beta > 0$, g is a cubic-like function and w satisfies

$$R(v, w) = \eta v - \gamma w,$$

with $\eta, \gamma > 0$. The FHN gating model yields only a coarse approximation of a typical cardiac action potential, particularly in the plateau and repolarization phases. A better approximation is given by the following variant by Rogers and McCulloch [47]

$$I_{ion}(v,w) = Gv\left(1-\frac{v}{v_{th}}\right)\left(1-\frac{v}{v_p}\right)+\eta_1 vw,$$
$$\frac{\partial w}{\partial t} = \eta_2\left(\frac{v}{v_p}-\eta_3 w\right),$$

where $G, \eta_1, \eta_2, \eta_3$ are positive real coefficients, v_{th} is a threshold potential and v_p the peak potential. We will consider this variant as our simplest gating model. The action potential generated with this model is plotted in the left panel of Figure 4.1 (continuous line), together with the recovery variable w magnified by a factor 100 (dash-dotted line). A more recent simplified ionic model with three currents and two gating variables was extensively investigated by Fenton and Karma [20].

5. Variational formulation and mathematical analysis. In this section, we briefly describe the variational formulation of both the Monodomain and the Bidomain model, providing some references to their theoretical analysis.

Let V be the Sobolev space $H^1(\Omega)/R$ and define by

$$(\varphi,\psi) = \int_\Omega \varphi\psi \,\mathrm{dx}, \qquad \forall \varphi,\psi \in L^2(\Omega)$$
$$a_{i,e}(\varphi,\psi) = \int_\Omega (\nabla\varphi)^T D_{i,e}(\mathbf{x})\,\nabla\psi \,\mathrm{dx}, \quad a(\varphi,\psi) = \int_\Omega (\nabla\varphi)^T D(\mathbf{x})\,\nabla\psi \,\mathrm{dx} \quad \forall \varphi,\psi \in H^1(\Omega)$$

the usual L^2-inner product and elliptic bilinear forms. The variational formulation of the Monodomain model (3.1) reads as follows. Given $v_0, w_0 \in L^2(\Omega)$, $I_{app} \in L^2(\Omega\times(0,T))$, find $v \in W^{1,1}(0,T;V)$ and $w \in W^{1,1}(0,T;L^2(\Omega)^M)$ such that $\forall t \in (0,T)$

$$\text{(5.1)} \quad \begin{cases} \chi C_m \dfrac{\partial}{\partial t}(v(t),\varphi) + a(v(t),\varphi) + \chi(I_{ion}(v,w),\varphi) = (I_{app},\varphi) & \forall \varphi \in V \\ \dfrac{\partial}{\partial t}(w(t),\psi) = (R(v(t),w(t)),\psi) & \forall \psi \in L^2(\Omega)^M, \end{cases}$$

with appropriate initial conditions (2.3) on v, w.

Analogously, the variational formulation of the Bidomain model (2.2) reads as follows. Given $v_0, w_0 \in L^2(\Omega)$, $I^{i,e}_{app} \in L^2(\Omega\times(0,T))$, find $u_{i,e} \in L^2(0,T;V)$ and $w \in L^2(0,T;L^2(\Omega)^M)$ such that $\frac{\partial v}{\partial t} \in L^2(0,T;V)$, $\frac{\partial w}{\partial t} \in L^2(0,T;L^2(\Omega)^M)$, and $\forall t \in (0,T)$

$$\text{(5.2)} \quad \begin{cases} \chi C_m \dfrac{\partial}{\partial t}(v(t),\hat{u}_i) + a_i(u_i(t),\hat{u}_i) + \chi(I_{ion}(v,w),\hat{u}_i) = (I^i_{app},\hat{u}_i) & \forall \hat{u}_i \in V \\ -\chi C_m \dfrac{\partial}{\partial t}(v(t),\hat{u}_e) + a_e(u_e(t),\hat{u}_e) - \chi(I_{ion}(v,w),\hat{u}_e) = -(I^e_{app},\hat{u}_e) & \forall \hat{u}_e \in V \\ \dfrac{\partial}{\partial t}(w(t),\hat{w}) = (R(v(t),w(t)),\hat{w}), \quad v(\mathbf{x},t) = u_i(\mathbf{x},t) - u_e(\mathbf{x},t) & \forall \hat{w} \in L^2(\Omega)^M, \end{cases}$$

with initial conditions (2.3) on v, w and the compatibility condition (2.4) on $I^{i,e}_{app}$.

Many well-known theoretical results available for reaction-diffusion equations (see e.g. Britton [9] and Smoller [53]) can be applied to the Monodomain model. Less is known on degenerate reaction-diffusion systems such as the Bidomain model. For the Bidomain system with the FHN model, we refer to Colli-Franzone and Savaré [17] for existence, uniqueness and regularity results, both at the continuous and at the semidiscrete level, and to Sanfelici [51] for a convergence analysis of finite element approximations. A recent mathematical

analysis of the Bidomain model with more general gating systems can be found in Veneroni [59].

More results are known on the related eikonal approximation describing the propagation of the excitation front; we refer to Colli-Franzone et al. [12, 13], Keener [28] and Bellettini et al. [8]. A mathematical analysis of the Bidomain model using Γ-convergence theory can be found in Ambrosio et al. [4].

6. Finite element discretization in space. We will use hexahedral isoparametric Q_1 finite elements in space; see e.g. Quarteroni and Valli [45] for a general introduction to the finite element method. Our domain Ω representing the left ventricle is modeled by a family of truncated ellipsoids described by the parametric equations

$$\left\{\begin{array}{ll} x = a(r)\cos\theta\cos\phi & \phi_{min} \le \phi \le \phi_{max}, \\ y = b(r)\cos\theta\sin\phi & \theta_{min} \le \theta \le \theta_{max}, \\ z = c(r)\sin\theta & 0 \le r \le 1, \end{array}\right. \tag{6.1}$$

where $a(r) = a_1 + r(a_2 - a_1)$, $b(r) = b_1 + r(b_2 - b_1)$, $c(r) = c_1 + r(c_2 - c_1)$, and $a_i, b_i, c_i, i = 1, 2$ are given coefficients determining the main axes of the ellipsoid. As in [13], the fibers rotate intramurally linearly with the depth for a total amount of 120^o proceeding counterclockwise from epicardium to endocardium; see Figure 2.1. More precisely, in a local ellipsoidal reference system $(\mathbf{e}_\phi, \mathbf{e}_\theta, \mathbf{e}_r)$, the fiber direction $\mathbf{a}_l(\mathbf{x})$ at a point $\mathbf{x}$ is given by

$$\mathbf{a}_l(\mathbf{x}) = \mathbf{e}_\phi \cos\alpha(r) + \mathbf{e}_\theta \sin\alpha(r), \quad \text{with} \quad \alpha(r) = \frac{2}{3}\pi(1-r) - \frac{\pi}{4}, \qquad 0 \le r \le 1.$$

To take into account the obliqueness of $\mathbf{a}_l$ with respect to the ellipsoidal surfaces, we introduce, beside $\alpha(r)$, the "oblique" angle β (known as imbrication angle) which describes the deviation of $\mathbf{a}_l$ from the tangent position. For more details about the imbrication angle and the fiber pathways, see [13]. We also consider three-dimensional slabs of cardiac tissue, described in the usual cartesian coordinate system by

$$\left\{\begin{array}{l} x = a(r) \\ y = b(r) \\ z = c(r) \end{array}\right. \quad \text{with} \quad \left\{\begin{array}{l} \mathbf{a}_l(\mathbf{x}) = \mathbf{e}_x \cos\alpha(r) + \mathbf{e}_y \sin\alpha(r), \\ \alpha(r) = \alpha_0\pi(1-r) - \frac{\pi}{4}, \qquad 0 \le r \le 1. \end{array}\right. \tag{6.2}$$

The domain Ω is discretized by introducing a structured quasi-uniform grid of hexahedral isoparametric Q_1 elements obtained by a uniform subdivision of the intervals $[\phi_{min}, \phi_{max}]$, $[\theta_{min}, \theta_{max}]$, $[0, 1]$ into (n_ϕ, n_θ, n_r) subintervals. Using the same symbol Ω for the domain and its FEM approximation, we have $\Omega = \bigcup_{E \in \mathcal{T}_h} E$, where $E = T_E(\hat{E})$, with $\hat{E} = [-1, 1]^3$ and T_E a trilinear map. The associated finite element space is given by

$$V_h = \left\{ \varphi_h \in V : \varphi_h \text{ is continuous in } \Omega : \varphi_{h|_E} \circ T_E \in Q_1(\hat{E}),\ \forall E \in \mathcal{T}_h \right\},$$

where $Q_1(\hat{E})$ is the space of the trilinear functions on $\hat{E}$. A semidiscrete problem is obtained by applying a standard Galerkin procedure and choosing a finite element basis $\{\phi_i\}$ for V_h. Let $\mathrm{M} = (\mathrm{m}_{rs})$, $\mathrm{A} = (\mathrm{a}_{rs})$ and $\mathrm{A}_{i,e} = (\mathrm{a}^{i,e}_{rs})$ be the symmetric mass and stiffness matrices defined by

$$\mathrm{m}_{rs} = \sum_E \int_E \varphi_r\, \varphi_s \mathrm{dx},$$

$$\mathrm{a}_{rs} = \sum_E \int_E (\nabla\varphi_r)^T D(\mathbf{x})\, \nabla\varphi_s \mathrm{dx}, \quad \mathrm{a}^{i,e}_{rs} = \sum_E \int_E (\nabla\varphi_r)^T D_{i,e}(\mathbf{x})\, \nabla\varphi_s \mathrm{dx}.$$

Numerical quadrature with a simple trapezoidal rule in three dimensions is used in order to compute these integrals. Let $\mathrm{I}^h_{ion}, \mathrm{I}^h_{app}, \mathrm{I}^{i,h}_{app}, \mathrm{I}^{e,h}_{app}$ be the finite element interpolants of

$I_{ion}, I_{app}, I^i_{app}, I^e_{app}$, respectively. In the following, we will denote by the same letters finite element functions and the vectors of their nodal values. In the Monodomain model, the finite element approximation $\mathbf{v}_h$ of the transmembrane potential is the solution of

$$\chi C_m \mathrm{M} \frac{\partial \mathbf{v}_h}{\partial t} + \mathrm{A}\mathbf{v}_h + \chi \mathrm{M}\, \mathrm{I}^h_{ion}(\mathbf{v}_h, \mathbf{w}_h) = \mathrm{M}\, \mathrm{I}^h_{app}, \tag{6.3}$$

while in the Bidomain model, the finite element approximations $\mathbf{u}_{i,h}, \mathbf{u}_{e,h}$ of the intra ed extracellular potentials are the solutions of the system

$$\begin{cases} \chi C_m \mathrm{M} \dfrac{\partial \mathbf{v}_h}{\partial t} + \mathrm{A}_i \mathbf{u}_{i,h} + \chi \mathrm{M}\, \mathrm{I}^h_{ion}(\mathbf{v}_h, \mathbf{w}_h) = \mathrm{M}\, \mathrm{I}^{i,h}_{app} \\ \\ -\chi C_m \mathrm{M} \dfrac{\partial \mathbf{v}_h}{\partial t} + \mathrm{A}_e \mathbf{u}_{e,h} - \chi \mathrm{M}\, \mathrm{I}^h_{ion}(\mathbf{v}_h, \mathbf{w}_h) = -\mathrm{M}\, \mathrm{I}^{e,h}_{app}, \end{cases} \tag{6.4}$$

where $\mathbf{v}_h = \mathbf{u}_{i,h} - \mathbf{u}_{e,h}$. In both cases, these equations are coupled with the semidiscrete approximations of the gating and concentration system

$$\frac{\partial \mathbf{w}_h}{\partial t} = R(\mathbf{v}_h, \mathbf{w}_h).$$

The Bidomain system can be written in compact form as

$$\chi C_m \mathcal{M} \frac{\partial}{\partial t} \begin{pmatrix} \mathbf{u}_{i,h} \\ \mathbf{u}_{e,h} \end{pmatrix} + \mathcal{A} \begin{pmatrix} \mathbf{u}_{i,h} \\ \mathbf{u}_{e,h} \end{pmatrix} + \chi \begin{pmatrix} \mathrm{M}\mathrm{I}^h_{ion}(\mathbf{v}_h, \mathbf{w}_h) \\ -\mathrm{M}\mathrm{I}^h_{ion}(\mathbf{v}_h, \mathbf{w}_h) \end{pmatrix} = \begin{pmatrix} \mathrm{M}\mathrm{I}^{i,h}_{app} \\ -\mathrm{M}\mathrm{I}^{e,h}_{app} \end{pmatrix}, \tag{6.5}$$

where

$$\mathcal{M} = \begin{bmatrix} \mathrm{M} & -\mathrm{M} \\ -\mathrm{M} & \mathrm{M} \end{bmatrix}, \quad \mathcal{A} = \begin{bmatrix} \mathrm{A}_i & 0 \\ 0 & \mathrm{A}_e \end{bmatrix}.$$

The Bidomain system (6.4) can alternatively be written in terms of $\mathbf{v}_h, \mathbf{u}_{e,h}$ by adding the two equations and substituting $\mathbf{u}_{i,h} = \mathbf{v}_h + \mathbf{u}_{e,h}$ into the first equation, obtaining

$$\begin{cases} \chi C_m \mathrm{M} \dfrac{\partial \mathbf{v}_h}{\partial t} + \mathrm{A}_i \mathbf{v}_h + \mathrm{A}_i \mathbf{u}_{e,h} + \chi \mathrm{M}\, \mathrm{I}^h_{ion}(\mathbf{v}_h, \mathbf{w}_h) = \mathrm{M}\, \mathrm{I}^{i,h}_{app} \\ \\ \mathrm{A}_i \mathbf{v}_h + (\mathrm{A}_e + \mathrm{A}_i)\mathbf{u}_{e,h} = \mathrm{M}(\mathrm{I}^{i,h}_{app} - \mathrm{I}^{e,h}_{app}). \end{cases} \tag{6.6}$$

In the language of Differential-Algebraic equations (DAE), this formulation separates the differential variable ($\mathbf{v}_h$) from the algebraic variable ($\mathbf{u}_{e,h}$); it was first used in [48, 12] and subsequently by many others, e.g. [26, 27, 10, 24, 29, 34, 55, 58]. Finally, another numerical approach [43, 21] has been recently applied to the Monodomain model using a splitting of the diffusion and reaction operators.

7. Semi-implicit time discretization. From the point of view of the time discretization, a main structural difference between the Bidomain and Monodomain model is that the mass matrix M of the latter is nonsingular, while the mass matrix $\mathcal{M}$ of the former is singular. This fact prevents the construction of any fully explicit method for the Bidomain model. One of our main goals is the simulation of a full normal heartbeat, consisting in three distinct spatio-temporal phases. First, in the excitation phase, a small time step Δt is required to accurately approximate the upstroke of the action potential. Subsequently, a larger Δt is allowed in the plateau phase and finally an intermediate Δt is needed for the smooth downstroke of the action potential. The use of an implicit treatment of the diffusion terms in (6.3) and (6.4) is needed in order to avoid a stability constraint on Δt induced by the fine mesh size h. This allows to adaptively change the time step according to the stiffness of the reaction term related to the main three phases of the heartbeat.

Therefore, we consider a semi-implicit method where the diffusion term is discretized by the implicit Euler method, while the nonlinear reaction term I_{ion} is treated explicitly; see Ascher et al. [5]. More expensive fully implicit methods are possible, see Hooke [26], Pormann [42]. The mass matrix M is approximated by a standard lumping technique in order to reduce it to diagonal form. The ODE system for the gating and concentration variables is discretized by the semi-implicit Euler method. In this way we decouple the ODE system by solving for the gating and concentration variables first (given the potential $\mathbf{v}^n$ at the previous time step)

$$\frac{\mathbf{w}^{n+1}-\mathbf{w}^n}{\Delta t} = R(\mathbf{v}^n, \mathbf{w}^{n+1})$$

and then solving for $\mathbf{v}^{n+1}$ in the Monodomain case

$$\chi C_m \mathrm{M}\frac{\mathbf{v}^{n+1}-\mathbf{v}^n}{\Delta t} + \mathrm{A}\mathbf{v}^{n+1} + \chi \mathrm{M}\,\mathrm{I}^h_{ion}(\mathbf{v}^n, \mathbf{w}^{n+1}) = \mathrm{M}\,\mathrm{I}^h_{app}, \tag{7.1}$$

or for $\mathbf{u}_i^{n+1}, \mathbf{u}_e^{n+1}$ in the Bidomain case

$$\begin{cases} \chi C_m \mathrm{M}\dfrac{\mathbf{v}^{n+1}-\mathbf{v}^n}{\Delta t} + \mathrm{A}_i\mathbf{u}_i^{n+1} + \chi \mathrm{M}\,\mathrm{I}^h_{ion}(\mathbf{v}^n, \mathbf{w}^{n+1}) = \mathrm{M}\,\mathrm{I}^{i,h}_{app} \\ -\chi C_m \mathrm{M}\dfrac{\mathbf{v}^{n+1}-\mathbf{v}^n}{\Delta t} + \mathrm{A}_e\mathbf{u}_e^{n+1} - \chi \mathrm{M}\,\mathrm{I}^h_{ion}(\mathbf{v}^n, \mathbf{w}^{n+1}) = -\mathrm{M}\,\mathrm{I}^{e,h}_{app}, \end{cases} \tag{7.2}$$

where $\mathbf{v}^n = \mathbf{u}_i^n - \mathbf{u}_e^n$. Alternatively, one could solve for the potentials first (given the gating and concentration variables at the previous time step) and then solve for the new gating and concentration variables. The resulting semi-implicit iterative method in the Monodomain case (7.1) is

$$\left(\frac{\chi C_m}{\Delta t}\mathrm{M} + \mathrm{A}\right)\mathbf{v}^{n+1} = \frac{\chi C_m}{\Delta t}\mathrm{M}\mathbf{v}^n - \chi \mathrm{M}\,\mathrm{I}^h_{ion}(\mathbf{v}^n, \mathbf{w}^{n+1}) + \mathrm{M}\,\mathrm{I}^h_{app}, \tag{7.3}$$

while the Bidomain case (7.2) can be written, in terms of the iteration matrix, i.e. the weighted sum of mass and stiffness matrices, as

$$\left(\frac{\chi C_m}{\Delta t}\begin{bmatrix} \mathrm{M} & -\mathrm{M} \\ -\mathrm{M} & \mathrm{M} \end{bmatrix} + \begin{bmatrix} \mathrm{A}_i & 0 \\ 0 & \mathrm{A}_e \end{bmatrix}\right)\begin{pmatrix} \mathbf{u}_i^{n+1} \\ \mathbf{u}_e^{n+1} \end{pmatrix} = \tag{7.4}$$

$$\frac{\chi C_m}{\Delta t}\begin{bmatrix} \mathrm{M} & -\mathrm{M} \\ -\mathrm{M} & \mathrm{M} \end{bmatrix}\begin{pmatrix} \mathbf{u}_i^n \\ \mathbf{u}_e^n \end{pmatrix} - \chi\begin{pmatrix} \mathrm{M}\mathrm{I}^h_{ion}(\mathbf{v}^n, \mathbf{w}^{n+1}) \\ -\mathrm{M}\mathrm{I}^h_{ion}(\mathbf{v}^n, \mathbf{w}^{n+1}) \end{pmatrix} + \begin{pmatrix} \mathrm{M}\mathrm{I}^{i,h}_{app} \\ -\mathrm{M}\mathrm{I}^{e,h}_{app} \end{pmatrix}.$$

We assign the initial conditions $\mathbf{u}_i^0 = -84$ mV and $\mathbf{u}_e^0 = 0$ mV, so that $\mathbf{v}^0 = -84$ mV. As in the continuous model, $\mathbf{v}^n$ is uniquely determined by the given initial and boundary conditions, while $\mathbf{u}_i^n$ and $\mathbf{u}_e^n$ are determined only up to the same additive time-dependent constant related to a reference potential. Since we consider bounded domains, we can determine this constant by imposing the condition $\mathrm{M}\mathbf{u}_e^n = 0$.

We remark that this semi-implicit treatment leads to a linear system at each time step in (7.3) with a symmetric positive definite iteration matrix, while the linear system in (7.4) involves a symmetric positive semidefinite iteration matrix, with a one-dimensional kernel spanned by $(\mathbf{1}, \mathbf{1})^T$. These systems are solved iteratively by the preconditioned conjugate gradient (PCG) method, using as initial guess the solution at the previous time step. More details on the parallel linear solver are given in the next section. On the contrary, for the DAE formulation (6.4) in the $\mathbf{v}, \mathbf{u}_e$ variables, the implicit treatment of all the linear terms would yield a nonsymmetric iteration matrix; hence a more expensive Krylov space method such as GMRES should be used for solving the associated linear system at each

time step. Moreover, the extension of the recent Monodomain operator splitting techniques [43, 21] to the Bidomain model would lead to a linear parabolic system $\chi C_m \mathcal{M} \frac{\partial \mathbf{u}}{\partial t} + \mathcal{A}\mathbf{u} = 0$, with $\mathbf{u} = (\mathbf{u}_{i,h}, \mathbf{u}_{e,h})^T$. The iteration matrix arising from the implicit discretization of this system coincides with the iteration matrix in (7.4) and therefore we would have the same computational complexity at each time step.

The adaptive time-stepping strategy employed is based on controlling the transmembrane potential variation $\Delta v = max(\mathbf{v}^{n+1} - \mathbf{v}^n)$ at each time step; see Victorri et al. [60], Luo and Rudy [32], Hooke [26], Otani [36]. In short, the adaptive strategy is the following:

if $\Delta v < \Delta v_{min} = 0.05$ then $\Delta t_{new} = \dfrac{\Delta v_{max}}{\Delta v} \Delta t_{old}$ (if $\Delta t_{new} < \Delta t_{max} = 6$ msec);

if $\Delta v > \Delta v_{max} = 0.5$ then $\Delta t_{new} = \dfrac{\Delta v_{min}}{\Delta v} \Delta t_{old}$ (if $\Delta t_{new} > \Delta t_{min} = 0.005$ msec).

Due to the linearity of the gating equation for $\mathbf{w}_j$, in the Hodgkin-Huxley formalism the equations can be written as

$$\begin{cases} \dfrac{\partial \mathbf{w}_j}{\partial t} = \dfrac{\mathbf{w}_{j\infty} - \mathbf{w}_j}{\tau_{w_j}} \ , \quad \text{on}(0, \Delta t) \quad \text{, with} \quad \mathbf{w}_j(\mathbf{x}, 0) = \mathbf{w}_j^n(\mathbf{x}) \\ \mathbf{w}_{j\infty}(\mathbf{v}^n) = \alpha_j(\mathbf{v}^n) * \tau_{w_j}(\mathbf{v}^n), \quad \tau_{w_j}(\mathbf{v}^n) = \dfrac{1}{\alpha_j(\mathbf{v}^n) + \beta_j(\mathbf{v}^n)}. \end{cases}$$

In order to also guarantee a control on the variation of the gating variables $\mathbf{w}_j$, they are integrated exactly given $\mathbf{v}$ (see Victorri et el. [60]), i.e.

$$\mathbf{w}_j^{n+1} = \mathbf{w}_{j\infty}(\mathbf{v}^n) + (\mathbf{w}_j^n - \mathbf{w}_{j\infty}(\mathbf{v}^n)) * exp(-\Delta t / \tau_{w_j}(\mathbf{v}^n)).$$

In particular, in the LR1 ionic model, the update of the gating variables $w_1, \cdots, w_6$ are based on the previous explicit formula; using these values the calcium concentration w_7 is then updated applying the implicit Euler method.

8. Parallel implementation and computational costs. In order to reduce the high computational cost of large-scale simulations of the whole heartbeat solving (7.3) and (7.4) at each time step, we have chosen to use adaptive methods in time, described before, and parallel solvers in space. Among other works using parallel tools in cardiac simulations, see Saleheen et al. [50], Quan et al. [44], Pormann [42], Garfinkel et al. [21], Vigmon et al. [61]. Our strategy for building an efficient parallel solver is based on using the parallel library PETSc from Argonne National Laboratory; see [7, 6]. This library, built on the MPI standard, offers advanced data structures and routines for the parallel solution of partial differential equations, from basic vector and matrix operations to more complex linear and nonlinear equation solvers. In our FORTRAN code, the necessary vectors and matrices are built and subassembled in parallel on each processor and then the solution is advanced in time on each processor in a synchronous manner. In order to minimize the bandwidth of the stiffness matrix (as in [40, 26]) and to improve data locality in PETSc, we have reordered the unknowns writing for every node the $\mathbf{u}_i$ and $\mathbf{u}_e$ components consecutively. This allows us to take full advantage of the parallel objects in the PETSc library, such as the Distributed Arrays (DA) objects, where the couple $\mathbf{u}_i$, $\mathbf{u}_e$ is associated with each node of the structured mesh. At each time step, the main computational costs are associated with

a) updating the gating and concentration variables;

b) evaluating the reaction terms (and possibly auxiliary quantities such as the depolarization and repolarization times defined below);

c) solving a linear system, related to the implicit treatment of the anisotropic diffusion terms, with coefficient matrix given in (7.3) for the Monodomain model or in (7.4) for the Bidomain model. As it is shown by the numerical experiments described in the next section, the iterative solution of this linear system is much harder for the Bidomain model than for the Monodomain model. This fact seems due to the more severe ill-conditioning of the Bidomain matrix related to its degenerate structure rather than just to the size doubling of the unknowns. The addition to the stiffness matrix A and $\mathcal{A}$ (related to elliptic operators

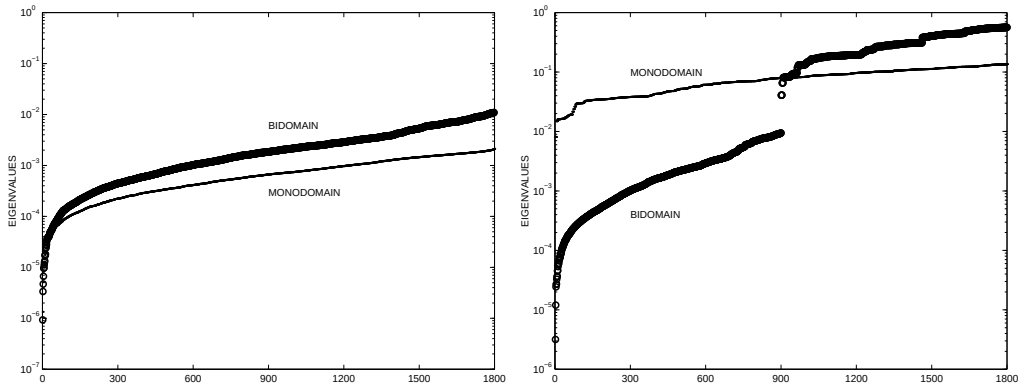

FIG. 8.1. *Nonzero eigenvalues of the stiffness matrices* A *and* $\mathcal{A}$ *related to elliptic operators with homogeneous Neumann boundary conditions (left panel) and of the iteration matrices in (7.3) and (7.4) (right panel). Monodomain eigenvalues, denoted by dots (·), are related to* $15 \times 15 \times 8 = 1800$ *meshpoints. Bidomain eigenvalues, denoted by circles (o), are related to* $15 \times 15 \times 4$ *meshpoints.*

with Neumann boundary conditions) of a zero-order term with the mass matrix, stemming from the time stepping scheme, greatly improves the spectrum of the Monodomain iteration matrix $\frac{\chi C_m}{\Delta t}\mathrm{M} + \mathrm{A}$ in (7.3), but not of the Bidomain iteration matrix $\frac{\chi C_m}{\Delta t}\mathcal{M} + \mathcal{A}$ in (7.4); see Figure 8.1 for a plot of the spectra of these matrices on a small 15×15×8 mesh in the Monodomain case and 15×15×4 in the Bidomain case (we chose these meshes in order to have iteration matrices of the same size).

Since the resulting matrices are symmetric positive definite (in the Monodomain case) or positive semidefinite (in the Bidomain case), we used the preconditioned conjugate gradient methods (PCG); see Demmel et al. [18]. In the Bidomain case, the constraint (2.5) related to the chosen reference potential, is enforced at each time step by shifting the PCG solution so that $\mathbf{1}^T \mathrm{M}\mathbf{u}_e^n = 0$. The iteration is stopped when the l_2-norm of the residual is less than 10^{-4}. We used a block Jacobi preconditioner with ILU(0) solver on each block. The blocks are associated with a decomposition of the domain Ω into subdomains and each one is assigned to one processor. This one-level preconditioner is not optimal, since from the theory developed for linear elliptic problems we known that the number of iterations of the resulting solver will depend on the number of subdomains. A two-level preconditioner, with an additional coarse solver associated with the coarse subdomain mesh, would produce an optimal preconditioner, but it would also increase the cost of each iteration; see Smith et al. [52]. Our numerical results show that for the Monodomain model the number of iterations of the one-level preconditioner is quite satisfactory, while for the Bidomain model the number of iterations increases considerably with the number of subdomains. Therefore more research is needed in order to build a more scalable Bidomain solver. We are currently working on the implementation of a two-level preconditioner.

9. Numerical results. We have conducted several numerical experiments in three dimensions on distributed memory parallel architectures, with both the Monodomain and the Bidomain model and different membrane models. The parallel machines employed are an IBM SP RS/6000 Power4 of the Cineca Consortium (www.cineca.it) and an HP SuperDome 64000 of the Cilea Consortium (www.cilea.it). The IBM SP machine has 512 processors Power 4 - 1300 MHz, grouped into 16 nodes of 32 processors and 64 GB RAM each. Its peak performance is declared at 2.7 Tflops, but we could not get more than 128 processors due to contention with other users. The HP SuperDome machine has 64 processors PA8700 - 750 MHz and 64 GB RAM.

In order to describe the macroscopic features of the excitation and subsequent repolarization process, we extract from the spatio-temporal transmembrane potential the sequence of the propagating excitation and repolarization wave fronts. During the excitation phase

TABLE 9.1
Parameters calibration for numerical tests

ellipsoidal geometry	$a_1 = b_1 = 1.5\ cm,\quad a_2 = b_2 = 2.7\ cm,\quad c_1 = 4.4,\quad c_2 = 5\ cm$ $\phi_{min} = 0,\quad \phi_{max} = 2\pi,\quad \theta_{min} = -3\pi/8,\quad \theta_{max} = \pi/8$
	$\chi = 10^3\ cm^{-1},\quad C_m = 10^{-3}\ mF/cm^2$
Monodomain parameters	$\sigma_l = 1.2 \cdot 10^{-3}\ \Omega^{-1}cm^{-1},\quad \sigma_t = 2.5562 \cdot 10^{-4}\ \Omega^{-1}cm^{-1}$ $G = 1.5\ \Omega^{-1}cm^{-2},\quad v_{th} = 13\ mV,\quad v_p = 100\ mV$ $\eta_1 = 4.4\ \Omega^{-1}cm^{-2},\quad \eta_2 = 0.012,\quad \eta_3 = 1$
Bidomain parameters	$\sigma_l^e = 2 \cdot 10^{-3}\ \Omega^{-1}cm^{-1},\quad \sigma_l^i = 3 \cdot 10^{-3}\ \Omega^{-1}cm^{-1}$ $\sigma_t^e = 1.3514 \cdot 10^{-3}\ \Omega^{-1}cm^{-1},\quad \sigma_t^i = 3.1525 \cdot 10^{-4}\ \Omega^{-1}cm^{-1}$ $\sigma_n^e = \sigma_t^e/\mu_1,\quad \sigma_n^i = \sigma_t^i/\mu_2$ $\mu_1 = \mu_2 = 1$ axial isotropic case, $\quad \mu_1 = 2, \mu_2 = 10$ orthotropic case

$v(\cdot, t)$ increases monotonically from the resting value v_r, see Figure 4.1, hence choosing a threshold $v^\star > v_r$ and lower than the plateau value, there is a unique time instant $t_e(\mathbf{x})$ when $v(\mathbf{x}, t_e(\mathbf{x})) = v^\star$. Analogously, during the repolarization phase there is a unique time instant $t_r(\mathbf{x})$ when $v(\mathbf{x}, t_r(\mathbf{x})) = v^\star$. In the following, we call t_e and t_r depolarization and repolarization times, respectively and their level surfaces (isochrones) define the excitation and repolarization wave fronts. We have chosen $v^\star = 56.5$ mV when using variants of FHN gating and $v^\star = -60$ mV when using LR1 gating. We remark that during the cardiac excitation phase a moving internal layer about 1 mm thick, associated to a fast variation of the transmembrane potential distribution v, sweeps the entire tissue. Therefore the computation on a fixed mesh requires a quasi uniform spatial resolution of the order of 0.1 mm in order to produce simulations free of numerical artifacts and sufficiently accurate.

9.1. Test 1: Monodomain model with a variant of FHN gating. We start with our simplest model, the Monodomain model with FHN gating; the details of the parameter calibration are given in Table 9.1 and the computing platform is the IBM SP4. The left ventricle geometry is modeled by a closed truncated ellipsoid, subdivided from 4 to 32 subdomains. The number of mesh points in each subdomain is kept fixed at 132×70×41 nodes, hence the global mesh (see Sect. 6) varies from 264×141×41 nodes in the smaller case with 4 subdomains (1.526.184 unknowns) to 1056×281×41 nodes in the larger case with 32 subdomains (12.166.176 unknowns). We simulated the depolarization of the ventricular volume after four stimuli of 250 mA/cm^3 have been applied for 1 msec on small areas (5 mesh points in each direction) of the epicardium. The model is run for 400 time steps of 0.2 msec each. At each time step, we compute the potential v, the recovery variable w and the depolarization time of the activated nodes.

In Figure 9.1, we plotted the isochrone lines of the depolarization time on three portions of the epicardial surface (anterior, lateral and posterior), showing the propagation and merging of the excitation fronts originating at each of the four stimulation sites, and on two transversal sections showing the intramural propagation of the fronts. The timings results reported in Table 9.2 show that the assembling times for the stiffness and mass matrices (fourth column) are reasonably small. The average number of PCG iterations per time step (fifth column) and the average timing per time step (last column) show the lack of scalability of the one-level block-Jacobi preconditioner, but for these numbers of processors these values are quite reasonable.

9.2. Test 2: Monodomain-LR1 model. We consider next the Monodomain equation with LR1 ionic model, simulating now the initial depolarization of some ellipsoidal blocks after one stimulus of 250 mA/cm^3 has been applied for 1 msec on a small area (5 mesh points in each direction) of the epicardium. The blocks are chosen in increasing sizes so as to keep constant the number of mesh points per subdomain (processor). As shown in Figure 9.2, the domain varies from the smaller block with 8 subdomains to half ventricle with 128 subdomains. We fixed the local mesh in each subdomain to be of 75×75×50 nodes

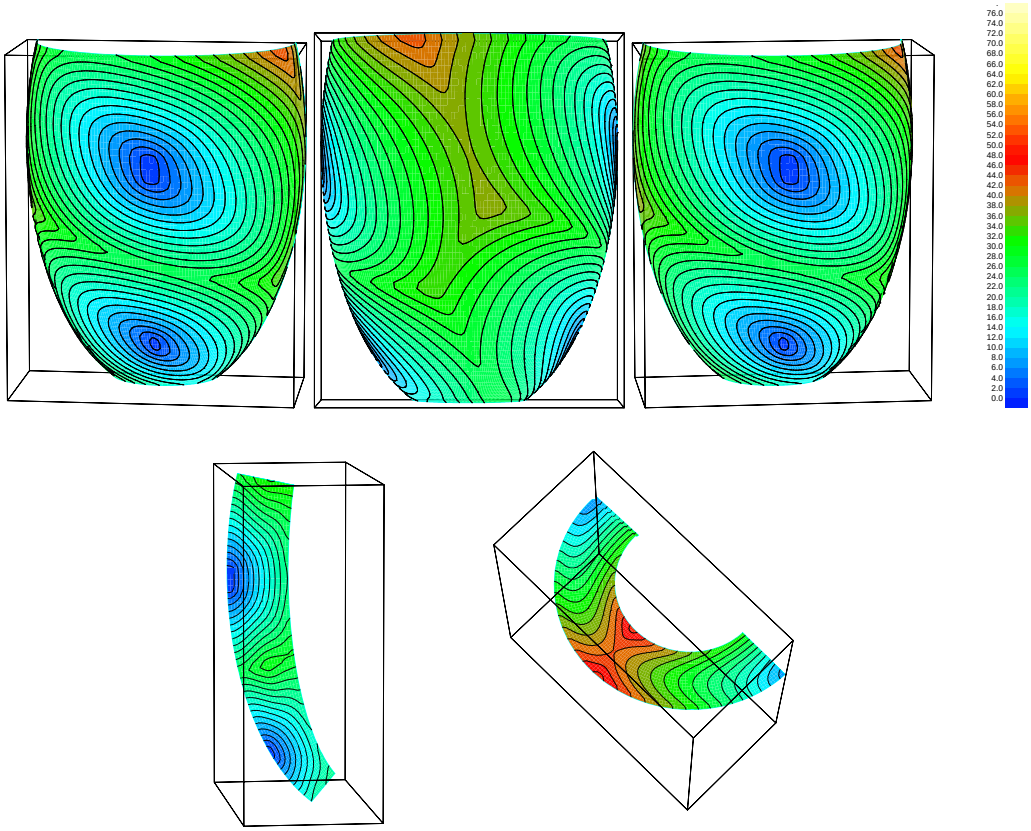

FIG. 9.1. *Test 1: Isochrones of the depolarization time drawn every 2 msec; anterior (top left), lateral (top center), posterior (top right) epicardial view, meridian section (bottom left), transverse section (bottom right). Colorbar values are in msec*

TABLE 9.2

Test 1: Monodomain with a variant of FHN model. Depolarization of full ventricle: 4 stimuli applied to the epicardial surface, 400 time steps of 0.2 msec each, computation of v,w and isochrones t_A = assembly timing, it = average number of PCG iterations at each time step, time = average CPU timing of each time step

# proc.	mesh	unknowns (nodes)	t_A	it.	time
4 = 2·2·1	264×141×41	1.526.184	10 s	10	3.5 s
9 = 3·3·1	396×211×41	3.425.796	11.2 s	12	5.9 s
16 = 4·4·1	528×281×41	6.083.088	11.1 s	14	8.6 s
32 = 8·4·1	1056×281×41	12.166.176	12.1 s	21	15 s

(281.750 unknowns), hence varying the global number of unknowns of the linear system from $2.25{\cdot}10^6$ in the smaller case with 8 subdomains on a global mesh of 150×150×100 nodes to $3.6{\cdot}10^7$ in the larger case with 128 subdomains on a global mesh of 600×600×100 nodes. The model is run for 30 time steps of 0.05 msec each. At each time step, we compute the potential v, the gating and concentration variables $w_1, \cdots, w_7$ and the depolarization time. The computing platform is the IBM SP4.

The results are reported in Table 9.3. The assembling time, average number of PCG iterations per time step and the average timing per time step (last three columns) are reasonably small and actually smaller than the results of Test 1, due to the smaller problem size per processor and time-step size. Up to 64 processors, the algorithm seems practically scalable, and even for 128 processors, the number of PCG iterations grows to just 8.

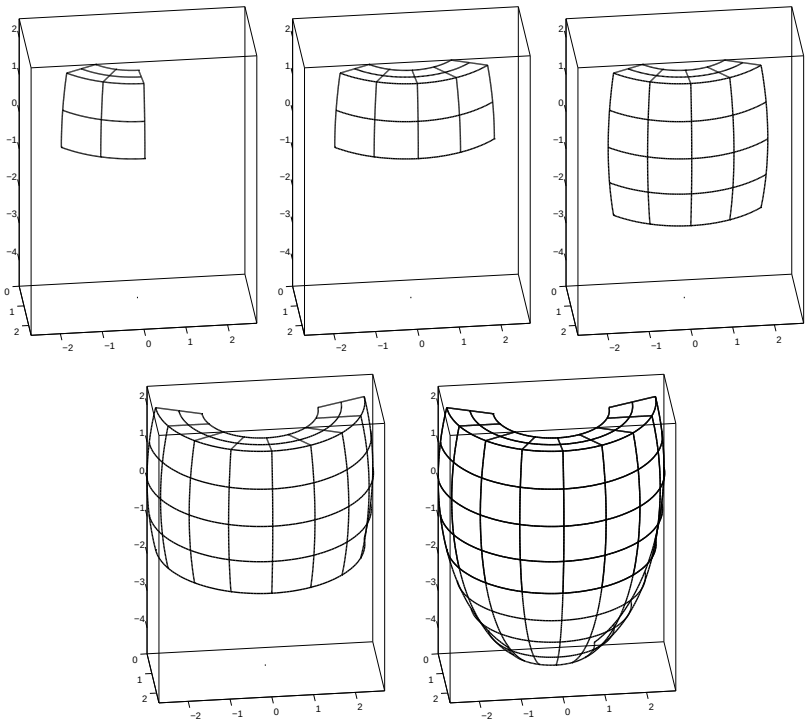

FIG. 9.2. *Domains for Tests 2 and 3: ellipsoidal blocks of increasing sizes decomposed into 8, 16, 32, 64 and 128 subdomains. Ellipsoidal geometry defined by (6.1) with parameters of Table 1. Axis thickmarks of the boxes are in centimeters*

TABLE 9.3
Test 2: Monodomain with LR1 model. Initial depolarization of an ellipsoidal block: 1 stimulus on epicardial surface, 30 time steps of 0.05 msec each, computation of $v, w_1, \cdots, w_7$ *and isochrones.* t_A = *assembly timing, it = average number of PCG iterations at each time step, time = average CPU timing of each time step*

# proc.	mesh	unknowns (nodes)	t_A	it.	time
$8 = 2{\cdot}2{\cdot}2$	150×150×100	2.250.000	7.7 s	4	2.7 s
$16 = 4{\cdot}2{\cdot}2$	300×150×100	4.500.000	8.5 s	4	3 s
$32 = 4{\cdot}4{\cdot}2$	300×300×100	9.000.000	9.1 s	5	3.6 s
$64 = 8{\cdot}4{\cdot}2$	600×300×100	18.000.000	9.2 s	5	3.6 s
$128 = 8{\cdot}8{\cdot}2$	600×600×100	36.000.000	10.6 s	8	5.1 s

The time spent by the solver in the LR1 membrane routine is about 1.4 sec. per time step and is independent on the global mesh size, since this routine is completely parallel (it depends of course on the local mesh size, here kept fixed). Therefore, its relative importance decreases as the problem size (and processor count) increases.

9.3. Test 3: Bidomain-LR1 model. We then consider the Bidomain system with LR1 ionic model, in the same setting (initial stimulus and domain decomposition) of the previous case. Due to the larger memory requirements of the Bidomain model, we used a smaller mesh of 50×50×35 nodes in each subdomain (processor), hence varying the global number of unknowns of the linear system from $1.4{\cdot}10^6$ in the smaller case with 8 subdomains on a global mesh of 100×100×70 to $2.24{\cdot}10^7$ unknowns in the larger case with 128 subdomains on a gloabl mesh of 400×400×70 nodes. As before, the model is run for 30 time steps of 0.05 msec each. At each time step, we now compute the potentials u_i, u_e, the gating and

TABLE 9.4

Test 3: Bidomain with LR1 model. Initial depolarization of an ellipsoidal block: 1 stimulus on epicardial surface, 30 time steps of 0.05 msec each, computation of $u_i, u_e, w_1, \cdots, w_7$ and isochrones. t_A = assembly timing, it = average number of PCG iterations at each time step, time = average CPU timing of each time step

# proc.	mesh	unknowns (2× nodes)	t_A	it.	time
8 = 2·2·2	100×100×70	1.400.000	12.9 s	98	40.2 s
16 = 4·2·2	200×100×70	2.800.000	13.3 s	127	55.5 s
32 = 4·4·2	200×200×70	5.600.600	15.7 s	148	72 s
64 = 8·4·2	400×200×70	11.200.000	16.2 s	176	91.9 s
128 = 8·8·2	400×400×70	22.400.000	18.4 s	244	129.7 s

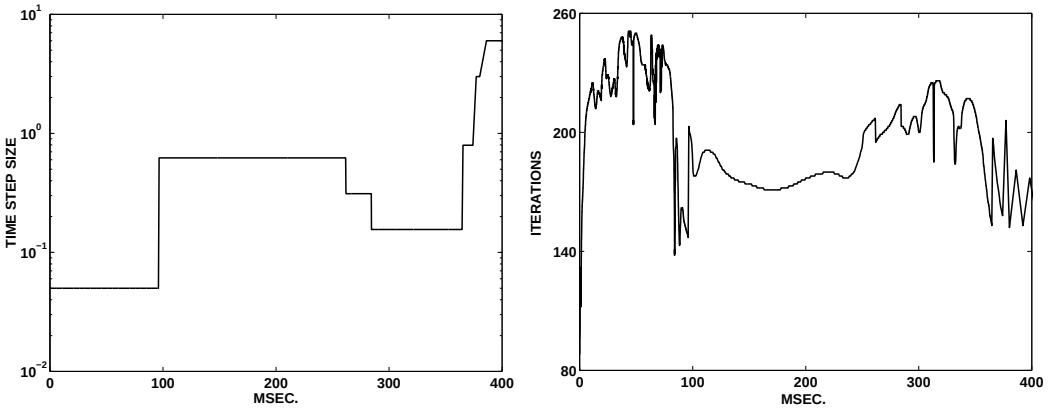

FIG. 9.3. *Test 4: Full cardiac cycle with Bidomain model and LR1 gating. Time-step size in msec. on a semilogarithmic scale (left), PCG iterations at each time step (right), both as a function of time*

concentration variables $w_1, \cdots, w_7$ and the depolarization time. The computing platform is the IBM SP4.

The results are reported in Table 9.4. While the assembling time remains reasonable (under 20 sec.), the average number of PCG iterations per time step and the average timing per time step are now much larger, clearly showing the limits of the one-level preconditioner and the effects of the severe ill-conditioning of the Bidomain iteration matrix. As shown in Figure 8.1, this iteration matrix displays a decay of the smallest eigenvalues similar to the stiffness matrix related to the elliptic operator with homogeneous Neumann boundary conditions. Therefore, we have applied the same solver to the linear system associated with the elliptic Neumann problem related to the tensor $D_i + D_e$, appearing as the algebraic part in the DAE formulation (6.6). The results show that the iteration counts are of the same order as those of Table 9.4. Hence, the loss of efficiency of our Bidomain solver is not due to the doubling of the unknown size and is also present in the DAE formulation where the algebraic system is half the size of the Bidomain system.

The time spent by the solver in the LR1 membrane routine is about 0.45 sec. per time step, independently of the global mesh size; the reduction with respect to the Monodomain case is due to the reduced local problem size.

9.4. Test 4: Full cardiac cycle with Bidomain-LR1 model. Knowledge of the rules that govern the full cardiac cycle, including excitation and repolarization processes, is a necessary prerequisite for understanding and interpreting abnormal sequences that occur in conduction disturbances, such as cardiac arrhythmias. However, while the excitation phase has been studied extensively, both experimentally and numerically, the repolarization phase remains incompletely understood; see Gotoh et al. [22], Cates and Pollard [10]. We now

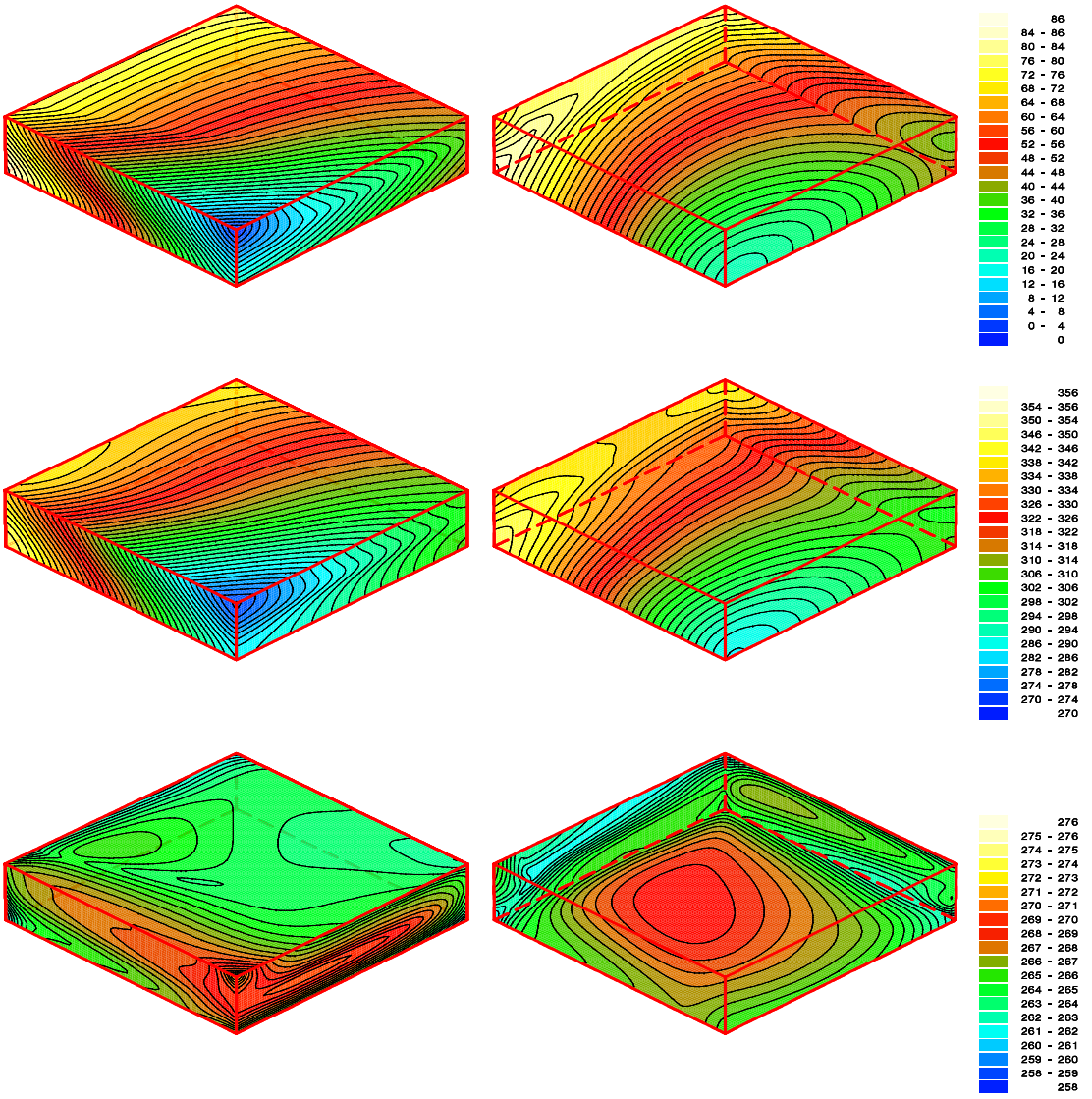

FIG. 9.4. *Test 4: Isochrones of the depolarization time (top row), repolarization time (center row) drawn every 2 msec and action potential duration (bottom row) drawn every 1 msec; front planes correspond to* $i = 1, j = 1, k = 51$ *(left), back planes correspond to* $i = 201, j = 201, k = 1$ *(right). Colorbar values are in msec.*

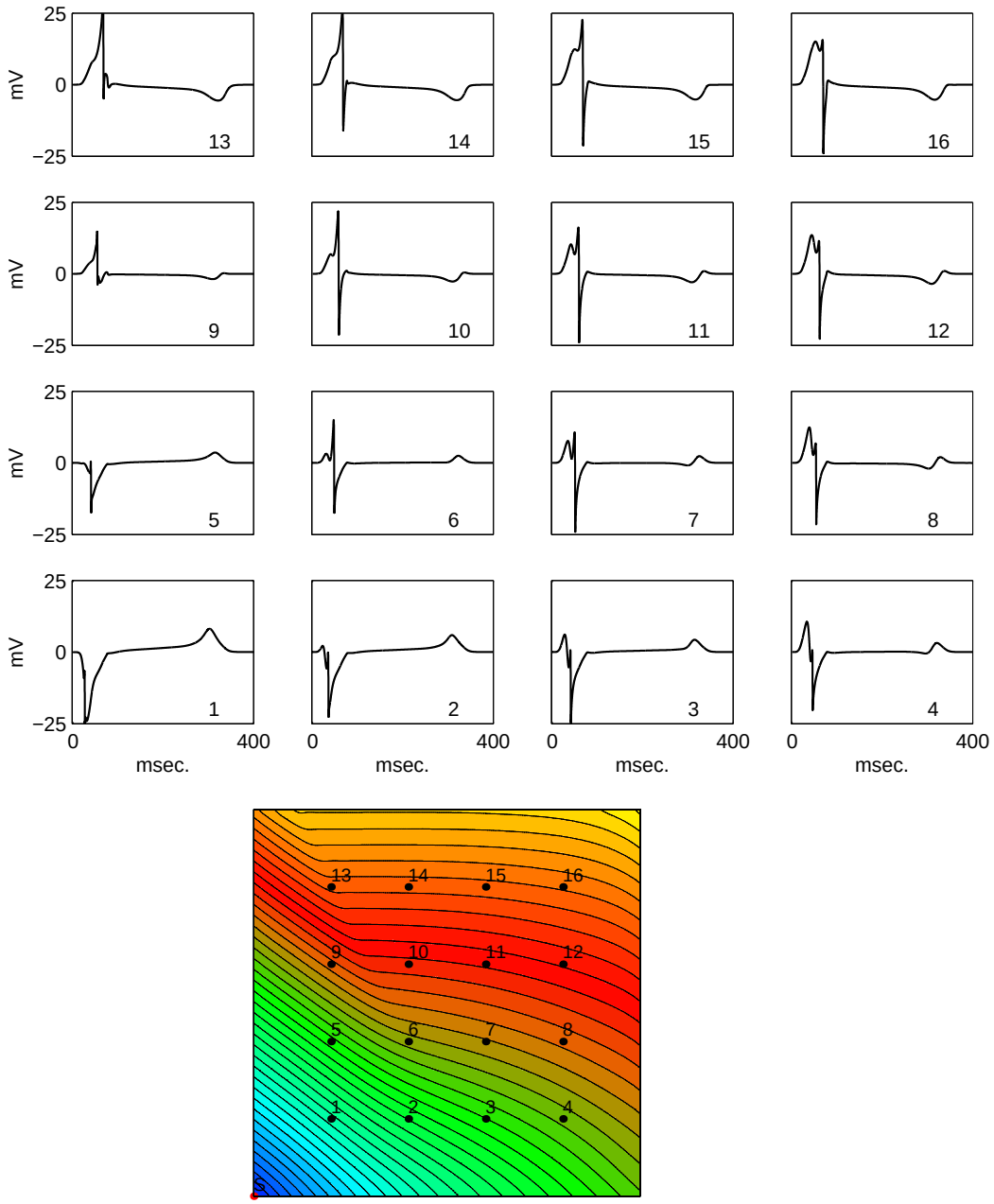

FIG. 9.5. *Test 4: plot in time of the extracellular potential u_e at the $4 \times 4 = 16$ points of the domain upper plane ($k = 51$) marked in the bottom panel.*

turn our attention to the simulation of the full cardiac cycle in a slab of cardiac tissue of size 2·2·0.5 cm^3, discretized with a fine mesh of 201×201×51 nodes. We use the Bidomain-LR1 model. The fibers rotate intramurally linearly with depth for a total amount of 90^o, i.e. $\alpha_0 = 0.5$ in (6.2). In this simulation, we assume a full orthotropic anisotropy with conductivity coefficients given in Table 9.1, $\mathbf{a}_n(\mathbf{x}) = \mathbf{e}_x \sin\alpha(r) - \mathbf{e}_y \cos\alpha(r)$ and $\mathbf{a}_t = \mathbf{e}_z$. The excitation process is started by applying a stimulus of 250 mA/cm^3 for 1 msec on a small area (3 mesh points in each direction) at a vertex of the slab.

Studies of the full cardiac cycle require much longer simulation time intervals, estimated by adding to the action potential duration (APD), which in the original LR1 model is more

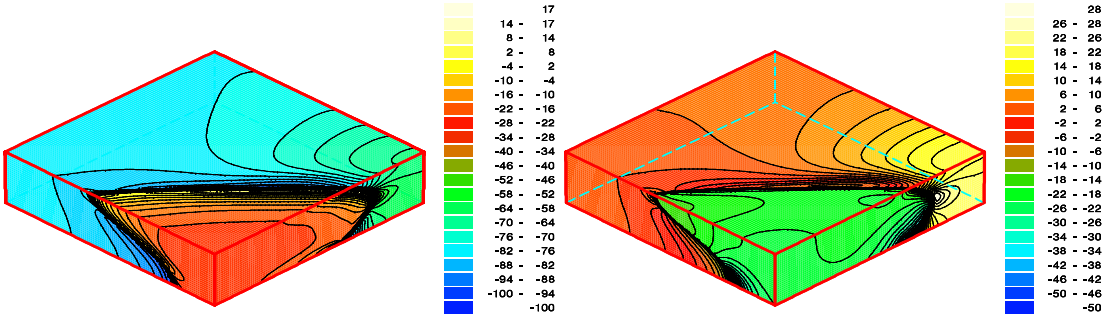

FIG. 9.6. *Test 4: isopotential lines of u_i (left) drawn every 3 mV and of u_e (right) drawn every 2 mV; time is 32 msec after stimulation. Colorbar values are in mV*

than 400 msec, the total excitation time related to the size of the cardiac volume. We scaled the slow inward current I_{si} of the LR1 model by a factor 2/3, thereby reducing the action potential duration to about 280 msec. Since the excitation of the entire slab in this test requires about 80 msec, the time interval for simulating the cardiac cycle is on the order of 400 msec. The adaptive time-stepping algorithm automatically adapts the time-step size in the different phases of the simulation. As shown in Figure 9.3, left panel, the initial small time step of 0.05 msec, needed while the steep depolarization front propagates throughout the domain, is increased to about 0.62 msec in the plateau phase, then decreased to 0.31 and 0.15 msec in the repolarization phase, and finally increased to the maximum size allowed of 6 msec when most of the tissue has returned to rest. Corresponding to these phases, the number of PCG iterations of the linear solver change considerably (right panel of Figure 9.3), increasing to a a maximum of about 250 iterations in the depolarization phase, decreasing to about 170 in the plateau phase, increasing again above 200 in the repolarization phase and finally decreasing below 160 when the tissue has returned to rest. This indicates that our preconditioner and/or initial guess are not yet satisfactory. This simulation of a full cardiac cycle of about 400 msec took about 6.4 days on the HP SuperDome machine with 25 processors.

The depolarization time $t_e(\mathbf{x})$, repolarization time $t_r(\mathbf{x})$ and action potential duration $t_r(\mathbf{x}) - t_e(\mathbf{x})$ (APD) are displayed in Figure 9.4. The propagation of the excitation and repolarization wave fronts is strongly affected by the anisotropic conduction and by the intramural fiber rotation. The third row of Figure 9.4 displays the dispersion of the APD. This large-scale computation is a first step toward a better understanding of how anisotropy affects the APD, contributing to its spatial heterogeneity; see e.g. the experimental studies by Gotoh et al. [22] and Taccardi et al. [57]. .

The waveforms of u_e, u_i and v are plotted in Figure 9.5 at the points indicated in the bottom right panel. The u_e waveforms (top left panel) display how the morphology of the QRS waves (related to the excitation phase) and of the T-wave (related to the recovery phase) changes as we move away from the stimulation site. We remark that the time adaptive

strategy efficiently computes these waveshapes without numerical artifacts such as spurious oscillations. Figure 9.6 displays the intra and extracellular potential distributions 32 msec after starting the stimulation, showing the very thin excitation layer, sweeping the domain and requiring a very small mesh size.

10. Conclusions. We have developed a portable parallel code for numerical simulations in computational electrocardiology in three dimensions. The code is based on the anisotropic Bidomain and Monodomain models describing the bioelectric process in the cardiac tissue. This model incorporates the main structural and functional features of the myocardium at a macroscopic level, i.e. the bidomain structure of the cardiac cellular aggregate, the anisotropic conductivity related to fibers assembling, the fiber rotation through the ventricular wall thickness, the laminar structure of the fiber architecture and the LR1 cellular membrane model, one of the most used in the literature. The FORTRAN code is based on structured isoparametric Q_1 finite elements in space and a semi-implicit adaptive method in time. Parallelization and portability are based on the PETSc parallel library. Large-scale simulations with up to $O(10^7)$ unknowns have been run on IBM SP4 and HP SuperDome parallel computers. We expect to be able to run simulations with $O(10^8)$ unknowns on machines with $O(10^3)$ processors. These simulations have shown that our numerical methods have a good performance when applied to the Monodomain model, even for a full left ventricular domain, while they need improvement in the Bidomain case, where a full heartbeat could be simulated only in a relatively small 3D block of tissue. The loss of efficiency in the Bidomain case is mostly related to the solution of the linear system at each time step and is shared by both the $\mathbf{u}_i, \mathbf{u}_e$ and the $\mathbf{v}, \mathbf{u}_e$ formulations. This is not only due to the doubling of the unknowns but can be attributed to the worst conditioning of the iteration matrix and to our preconditioning technique. On the other hand, it is well established by the agreement between experimental and simulated data that the bidomain structure cannot be neglected in modern simulation studies. Therefore, work is under way to develop more efficient elliptic solvers based on two-level domain decomposition methods and more efficient time advancement methods.

REFERENCES

[1] Special issue on *Fibrillation in normal ventricular myocardium. Chaos* 8 (1), 1998.
[2] Special issue on *Mapping and control of complex cardiac arrhythmias. Chaos* 12 (3), 2002.
[3] Special issue on *From excitable media to virtual cardiac tissue. Chaos Solit. Frac.* 13 (8), 2002.
[4] L. Ambrosio, P. Colli-Franzone and G. Savaré. On the asymptotic behaviour of anisotropic energies arising in the cardiac bidomain model. *Interfaces Free Bound.* 2 (3): 213–266, 2000.
[5] O. M. Ascher, S. J. Ruuth and B. T. R. Wetton. Implicit-explicit methods for time-dependent partial differential equations. *SIAM J. Numer. Anal.* 32 (3): 797–823, 1995.
[6] S. Balay, K. Buschelman, W. D. Gropp, D. Kaushik, M. Knepley, L. Curfman McInnes, B. F. Smith and H. Zhang. PETSc Users Manual. Tech. Rep. ANL-95/11 - Revision 2.1.5, Argonne National Laboratory, 2002.
[7] S. Balay, K. Buschelman, W. D. Gropp, D. Kaushik, M. Knepley, L. Curfman McInnes, B. F. Smith and H. Zhang. PETSc home page. http://www.mcs.anl.gov/petsc, 2001.
[8] G. Bellettini, P. Colli-Franzone and M. Paolini. Convergence of front propagation for anisotropic bistable reaction-diffusion equations. *Asymp. Anal.*, 15, 325–358, 1997.
[9] N. F. Britton. *Reaction-diffusion equations and their applications to biology.* Academic Press, London, 1986.
[10] A. W. Cates and A. E. Pollard. A model study of intramural dispersion of action potential duration in the canine pulmonary conus. *Ann. Biomed. Eng.* 26: 567–576, 1998.
[11] E. M. Cherry, H. S. Greenside and C. S. Henriquez. A space-time adaptive method for simulating complex cardiac dynamics *Phys. Rev. Lett.* 84 (6): 1343-1346, 2000.
[12] P. Colli Franzone, L. Guerri. Spread of excitation in 3-D models of the anisotropic cardiac tissue. **I**:Validation of the eikonal approach. *Math. Biosci.* 113:145-2 09, 1993.
[13] P. Colli Franzone, L. Guerri, M. Pennacchio, and B. Taccardi. Spread of excitation in 3-D models of the anisotropic cardiac tissue. **II**: Effects of fiber architecture and ventricular geometry. *Math. Biosci.* 147: 131–171, 1998.
[14] P. Colli Franzone, L. Guerri, M. Pennacchio, and B. Taccardi. Spread of excitation in 3-D models of the anisotropic cardiac tissue. **III**: Effects of ventricular geometry and fiber structure on the potential distribution. *Math. Biosci.* 151: 51–98, 1998.

[15] P. Colli Franzone, L. Guerri, M. Pennacchio and B. Taccardi. Anisotropic mechanisms for multiphasic unipolar electrograms. Simulation studies and experimental recordings. *Ann. Biomed. Eng.* 28: 1–17, 2000.

[16] P. Colli Franzone, M. Pennacchio and L. Guerri. Accurate computation of electrograms in the left ventricular wall. *Math. Mod. and Meth. in Appl. Sci.* M^3AS 10 (4): 507–538, 2000.

[17] P. Colli Franzone and G. Savaré. Degenerate evolution systems modeling the cardiac electric field at micro and macroscopic level. In *Evolution equations, Semigroups and Functional Analysis*, A. Lorenzi and B. Ruf, Editors, 49–78, Birkhauser, 2002.

[18] J. W. Demmel, M. T. Heath and H. A. van der Vorst. Parallel numerical linear algebra. *Acta Numerica* 111–197, 1993.

[19] I. R. Efimov, B. Ermentrout, D. T. Huang, and G. Salama. Activation and repolarization patterns are governed by different structural characteristics of ventricular myocardium: experimental study with voltage-sensitive dyes and numerical simulations. *J. Cardiovasc. Electrophysiol.* 7: 512–530, 1996.

[20] F. H. Fenton and A. Karma. Vortex dynamics in three-dimensional continuous myocardium with fiber rotation: filament instability and fibrillation. *Chaos* 8: 20–47, 1998.

[21] A. Garfinkel, Y-H. Kim, O. Voroshilovsky, Z. Qu, J. R. Kil, M-H. Lee, H. S. Karagueuzian, J. N. Weiss and P-S. Chen. Preventing ventricular fibrillation by flattening cardiac restitution. *Proc. Nat. Acad. Sci. USA* 97 (11): 6061-6066, 2000.

[22] M. Gotoh et al. Anisotropic repolarization in ventricular tissue. *Am. J. Physiol.* 41: 107–113, 1997.

[23] C. S. Henriquez. Simulating the electrical behavior of cardiac tissue using the bidomain model. *Crit. Rev. Biomed. Eng.* 21: 1–77, 1993.

[24] C. S. Henriquez, A. L. Muzikant and C. K. Smoak. Anisotropy, fiber curvature, and bath loading effects on activation in thin and thick cardiac tissue preparations: Simulations in a three-dimensional bidomain model. *J. Cardiovasc. Electrophysiol.* 7 (5): 424–444, 1996.

[25] A. L. Hodgkin and A. F. Huxley. A quantitative description of membrane current and its application to conduction and excitation in nerve. *J. Physiol.*, 117:500–544, 1952.

[26] N. Hooke. Efficient simulation of action potential propagation in a bidomain. Ph. D. Thesis, Duke Univ., Dept. of Comput. Sci., 1992.

[27] N. Hooke, C. S. Henriquez, P. Lanzkrom, and D. Rose. Linear algebraic transformations of the bidomain equations: implications for numerical methods. *Math. Biosc.* 120:127–145, 1994.

[28] J. P. Keener. An eikonal-curvature equation for the action potential propagation in myocardium, *J. Math Biol.* 29: 629–651, 1991.

[29] J. P. Keener and K. Bogar. A numerical method for the solution of the bidomain equations in cardiac tissue. *Chaos* 8 (1): 234–241, 1998.

[30] J. P. Keener and J. Sneyd. *Mathematical Physiology*. Springer-Verlag, New York 1998.

[31] I. J. LeGrice, B. H. Smaill, L. Z. Chai, S. G. Edgar, J. B. Gavin and P. J. Hunter. Laminar structure of the heart: ventricular myocyte arrangement and connective tissue architecture in the dog. *Am. J. Physiol. (Heart Circ. Physiol)*,269 (38): H571-H582, 1995.

[32] C. Luo and Y. Rudy. A model of the ventricular cardiac action potential: depolarization, repolarization, and their interaction. *Circ. Res.* 68 (6): 1501–1526, 1991.

[33] P. K. Moore. An adaptive finite element method for parabolic differential systems: some algorithmic considerations in solving in three space dimensions. *SIAM J. Sci. Comput.* 21 (4): 1567–1586, 2000.

[34] A. L. Muzikant, E. W. Hsu, P. D. Wolf and C. S. Henriquez. Region specific modeling of cardiac muscle: comparison of simulated and experimental potentials. *Ann. Biomed. Eng.* 30: 867–883, 2002.

[35] J. S. Neu and W. Krassowska. Homogenization of syncityal tissues. *Crit. Rev. Biom. Eng.* 21: 137–199, 1993.

[36] N. F. Otani. Computer modeling in cardiac electrophysiology. *J. Comput. Phys.* 161: 21–34, 2000.

[37] A. V. Panfilov. Spiral breakup as a model of ventricular fibrillation. *Chaos* 8 (1): 57-64, 1998.

[38] A. V. Panfilov and A. V. Holden. *Computational Biology of the Heart*. Wiley, 1997.

[39] M. Pennacchio. The mortar finite element method for the cardiac "bidomain" model of extracellular potential. *J. Sci. Comp.* To appear, 2003.

[40] M. Pennacchio and V. Simoncini. Efficient algebraic solution of reaction-diffusion systems for the cardiac excitation process. *J. Comput. Appl. Math.* 145 (1): 49–70, 2002.

[41] C. S. Peskin. Fiber architecture of the left ventricular wall: an asymptotic analysis. *Comm. Pure Appl. Math.* 42: 79–113, 1989.

[42] J. Pormann. A Simulation System for the Bidomain Equations. Ph. D. Thesis, Duke Univ., Dept. of Electr. Comput. Eng., 1999.

[43] Z. Qu and A. Garfinkel. An advanced algorithm for solving partial differential equation in cardiac conduction. *IEEE Trans. Biomed. Eng.* 46 (9): 1166–1168, 1997.

[44] W. Quan, S. J. Evans and H. M. Hastings. Efficient integration of a realistic two-dimensional cardiac tissue model by domain decomposition. *IEEE Trans. Biomed. Eng.* 45: 372–385, 1998.

[45] A. Quarteroni and A. Valli. *Numerical Approximation of Partial Differential Equations*. Springer-Verlag, Berlin, 1994.

[46] W. J. Rappel. Filament instability and rotational tissue anisotropy: A numerical study using detailed cardiac models. *Chaos* 11 (1): 71-80, 2001.

[47] J. M. Rogers and A. D. McCulloch. A collocation-Galerkin finite element model of cardiac action potential propagation. *IEEE Trans. Biomed. Eng.* 41: 743–757, 1994.
[48] B. J. Roth. Action potential propagation in a thick strand of cardiac muscle. *Circ. Res.* 68: 162–173, 1991.
[49] B. J. Roth. How the anisotropy of the intracellular and extracellular conductivities influence stimulation of cardiac muscle. *J. Math. Biol.* 30: 633–646, 1992.
[50] H. I. Saleheen and K. T. Ng. A new three-dimensional finite-difference bidomain formulation for inhomogeneous anisotropic cardiac tissues. *IEEE Trans. Biomed. Eng.* 45 (1): 15–25, 1998.
[51] S. Sanfelici. Convergence of the Galerkin approximation of a degenerate evolution problem in electrocardiology. *Numer. Meth. Part. Diff. Eq.* 18 (2): 218–240, 2002.
[52] B. F. Smith, P. Bjørstad, and W. D. Gropp, *Domain Decomposition: Parallel Multilevel Methods for Elliptic Partial Differential Equations*, Cambridge University Press, 1996.
[53] J. Smoller. *Shock waves and reaction-diffusion equations*. Springer-Verlag, New York, Second ed., 1994.
[54] D. Streeter. Gross morphology and fiber geometry in the heart. in *Handbook of Physiology*. Vol. 1, Sect. 2, pp. 61-112. R. M. Berne, Editor, Williams & Wilkins, 1979.
[55] J. Sudnes, G. T. Lines and A. Tveito. Efficient solution of ordinary differential equations modeling electrical activity in cardiac cells. *Math. Biosci.* 172: 55–72, 2003.
[56] B. Taccardi, E. Macchi, R.L. Lux, P.R. Ershler, S. Spaggiari, S. Baruffi, Y. Vyhmeister. Effect of myocardial fiber direction on epicardial potentials. *Circulation* 90:3076–3090, 1994.
[57] B. Taccardi, B. Punske. F. Helie, R. MacLeod, R. Lux, P. Ershler, T. Dustman and Y. Vyhmeister. Epicardial recovery sequences and excitation recovery intervals during paced beats. Role of myocardial architecture. *PACE* 22 (4) part II: 833, 1999.
[58] N. Trayanova, J. Eason and F. Aguel. Computer simulations of cardiac defibrillation: a look inside the heart. *Comput. Visual. Sci.* 4: 259–270, 2002.
[59] M. Veneroni. Il modello di Hodgkin-Huxley per la propagazione del campo elettrico cardiaco. *IMATI Tech. Rep.*, 2003, to appear.
[60] B. Victorri, A. Vinet, F. A. Roberge and J. P. Drouhard. Numerical integration in the reconstruction of cardiac action potentials using Hodgkin-Huxley type models. *Comp. Biomed. Res.* 18: 10–23, 1985.
[61] E. J. Vigmond, F. Aguel and N. A. Trayanova. Computational techniques for solving the bidomain equations in three dimensions. *IEEE Trans. Biomed. Eng.* 49 (11): 1260–1269, 2002.
[62] A. T. Winfree. Stable particle-like solutions to the nonlinear wave equations of three-dimensional excitable media. *SIAM Rev.* 32 (1): 1–53, 1990.
[63] A. T. Winfree. Electrical turbulence in three-dimensional heart muscle. *Science* 266 (5187): 1003–1006, 1994.
[64] H. Yu. Solving parabolic problems with different time steps in different regions in space based on domain decomposition methods. *Appl. Numer. Math.* 30 (4): 475–491, 1999.
[65] H. Yu. A local space-time adaptive scheme in solving two-dimensional parabolic problems based on domain decomposition methods. *SIAM J. Sci. Comput.* 23 (1): 304–322, 2001.
[66] D. Zipes and J. Jalife.*Cardiac Electrophysiology*. W. B. Sauders Co., Philadelphia, 2000.